Free-bound excitation and predissociation of ytterbium dimers near the math xmlns="http://www.w3.org/1998/Math/MathML">mrow>mmultiscripts>mi>S/mi>mn>0/mn>none>/none>mprescripts>/mprescripts>none>/none>mn>1/mn>/mmultiscripts>mtext>−/mtext>mmultiscripts>mi>P/mi>mn>1/mn>none>/none>mprescripts>/mprescripts>none>/none>mn>1/mn>/mmultiscripts>/mrow>/math> atomic transition

Katsunari Enomoto, Ryota Takabatake, Takehiro Suzuki, Yosuke Takasu, Yoshiro Takahashi, and Masaaki Baba

Phys. Rev. A **104**, 013118 — Published 30 July 2021

DOI: 10.1103/PhysRevA.104.013118

Free-bound excitation and predissociation of ytterbium dimers near the $^1S_0$-$^1P_1$ atomic transition

Katsunari Enomoto,[1] Ryota Takabatake,[1] Takehiro Suzuki,[1] Yosuke Takasu,[2] Yoshiro Takahashi,[2] and Masaaki Baba[3]

[1] *Department of Physics, Faculty of Science, University of Toyama, Toyama 930-8555, Japan*
[2] *Department of Physics, Graduate School of Science, Kyoto University, Kyoto 606-8502, Japan*
[3] *Department of Chemistry, Graduate School of Science, Kyoto University, Kyoto 606-8502, Japan*

(Dated: July 14, 2021)

A continuous excitation band of a free-bound photoassociation transition of ytterbium atoms is observed as a red wing of the $^1S_0$-$^1P_1$ atomic line at 399 nm for a hot thermal vapor. The excitation to the 0_u^+ molecular state is observed by monitoring fluorescence from the $^3P_1$ state atoms, which allows us to detect the production of Yb_2 molecules with high sensitivity. The photoassociation is characterized in comparison with transitions to atomic Rydberg states. The time profile of the fluorescence signal suggests that the 0_u^+ molecular state predissociates with states correlating to the $^1S_0$+$^3D_2$ atomic states.

I. INTRODUCTION

Ytterbium is a lanthanide element with an electronic configuration similar to those of alkaline-earth atoms. Ultracold Yb atoms have been utilized for various applications such as quantum simulations [1, 2] and atomic clocks [3–6]. One of the remarkable features of alkaline-earth(-like) atoms is the existence of metastable ($^3P_0$, $^3P_2$) states of long radiative lifetimes on the order of seconds or more. These states can also be employed in the above mentioned applications. Their collisional properties can be deduced from information on Yb_2 molecules. Certain molecular states are also used to probe the properties of atomic ensembles such as their density. It is therefore of growing importance to characterize both the electronic ground and excited states of Yb_2.

In spite of this need, spectroscopic data on Yb_2 is scarce, while there have been several spectroscopic studies on dimers of heavy alkaline-earth atoms (e.g. Sr [7–12] and Ba [13]) To the best of our knowledge, only one study using matrix isolation spectroscopy has observed absorption spectra of molecular transitions of Yb_2 with vibrational structures [14]. Quantum chemical calculations are also difficult for this heavy molecule. There have been theoretical studies of potential curves [15–19] and a breakdown of the Born-Oppenheimer approximation [20].

Recent studies have performed photoassociation spectroscopy of ultracold Yb atoms [21–31]. This type of spectroscopy can probe vibrational levels near the dissociation limit, and determine potential curves at long internuclear distances. For the $6s^2\ ^1S_0$-$6s6p\ ^1P_1$ transition at 398.9 nm, vibrational levels have been investigated up to the detuning of about 16 cm^{-1} from the dissociation limit [21, 23]. Not only the fact that Franck-Condon factors are smaller at deeper levels but also the line broadening that occurs due to predissociation prevents investigation at further detuning. The predissociation mechanism, whether the molecules dissociate to the $^1S_0$+^3P states or the $^1S_0$+^3D states, has not been determined through atom loss measurement [21].

In this paper we report our spectroscopy findings on a red wing of the $^1S_0$-$^1P_1$ atomic line using a thermal vapor of Yb. This wing corresponds to the photoassociation to the 0_u^+ molecular state correlating to the $^1S_0$+$^1P_1$ atomic state. Note that the term "photoassociation" used in this paper has the original meaning, the free-bound transition of an atomic pair, while nowadays it is typically used for narrow spectral signatures observed in ultracold atom experiments. Although rovibrational structure has not been resolved for this high-temperature photoassociation, our study was able to investigate a wide range of detuning up to about 150 cm^{-1}. The photoassociation was monitored via fluorescence at 555.6 nm from dissociated $^1S_0$+$^3P_1$ atomic pairs. The fluorescence from the relatively long-lived $^3P_1$ state was easy to distinguish in both wavelength and time domains from the background scattered light of a pulsed excitation laser beam. The predissociation mechanism was also clarified from the decay process to the $^1S_0$+$^3P_1$ state. A similar detection scheme has previously been employed for the predissociation of photoassociated ultracold potassium atoms [32].

There is a long history of studies on atomic line wings [33, 34]. Far wings of the $^1S_0$-$^1P_1$ transition of Yb atoms have been investigated for absorption spectra of Yb vapors in buffer gases [35, 36], and the wing due to the Yb-Yb collisions has been deduced by taking the limit of zero buffer-gas density [35]. The highly asymmetric spectrum that we report here, in contrast, was not obtained in that study, possibly due to differences between the detection schemes.

II. EXPERIMENT

Yb vapor was produced by heating pieces of Yb metal in a Type 316 stainless steel furnace. The furnace was heated to around 750 K by surrounding sheathed heaters. The temperature was measured by a thermocouple attached to the furnace. The vapor was extracted from the furnace into a vacuum space through an aperture 1.0 mm in diameter. In a typical iteration, 3 g of Yb metal

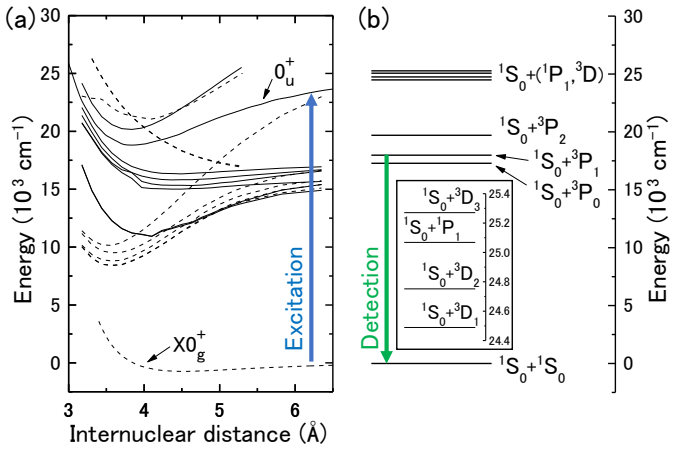

FIG. 1. Molecular and atomic energy level diagrams. (a) Potential energy curves of Yb_2 correlating to the $6s^2\ {}^1S_0$+($6s^2\ {}^1S_0$, $6s6p\ {}^1P_1$, $6s6p\ {}^3P$) atomic states. The curves of the $X0_g^+$, $0_u^+({}^1S_0+{}^1P_1)$, and the other states are traced from the graphs of Ref. [29], Ref. [15], and Ref. [19], respectively. Solid lines are for u states and dashed lines are for g states. Note that the curve of the $0_u^+({}^1S_0+{}^1P_1)$ state is shifted so that the asymptote coincides with the $^1S_0+{}^1P_1$ atomic level, while the curves of the other excited states are not shifted. (b) Energy levels of Yb atoms. The inset shows the levels around 25 000 cm^{-1}.

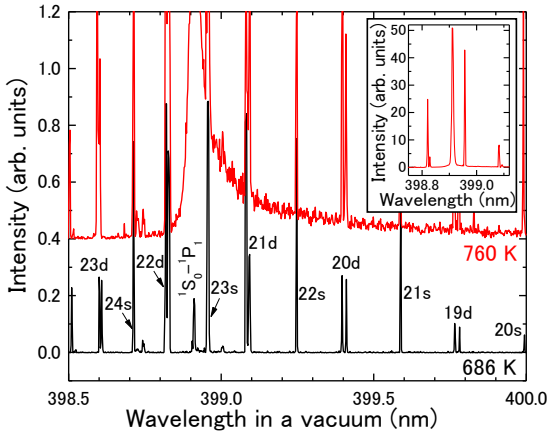

FIG. 2. Excitation spectra of Yb vapors obtained by monitoring the 555.6 nm fluorescence at two different temperatures shown with different offsets. The resonance line at 398.91 nm is the $^1S_0$-$^1P_1$ atomic transition, and the other sharp lines correspond to two-photon excitations to atomic Rydberg states. The labels indicate the assignment of atomic lines, e.g., 24s and 23d refer to the $6s24s\ {}^1S_0$ and $6s23d\ {}^{1,3}D_2$ states, respectively. For a $^{1,3}D_2$ doublet the longer wavelength line is the transition to the $^3D_2$ state. The broad continuous band observed at 760 K corresponds to the photoassociation of atomic pairs. The inset shows a part of the spectrum at 760 K with a large scale for the vertical axis.

was placed in the furnace, and the photoassociation signal was observed for several hours. The vacuum chamber was evacuated with a diffusion pump and a liquid nitrogen trap, and the pressure outside the furnace was about 0.01 Pa.

Yb atoms were excited by a pulsed dye laser positioned about 2 cm from the exit aperture of the furnace. An Exalite 404 dye laser was pumped by a XeCl excimer laser with a repetition rate of 10 Hz and a pulse duration of about 5 ns. The pulse energy of the dye laser was up to 0.3 mJ, and the laser beam cross section was about 6 mm^2. The wavelength of the dye laser was scanned around the $^1S_0$-$^1P_1$ atomic transition at 398.9 nm. There are four electronic states asymptotically connected to the $^1S_0+{}^1P_1$ atomic state (see Fig. 1): $0_u^+[{}^1\Sigma_u^+]$, $1_g[{}^1\Pi_g]$, $1_u[{}^1\Pi_u]$, and $0_g^+[{}^1\Sigma_g^+]$. All of these have potential energies of r^{-3} dependence at long internuclear distances r because of the resonant dipole interaction. The 0_u^+ and 1_g states are attractive at long r, while the 1_u and 0_g^+ states are repulsive. The 0_u^+ and 1_u states have dipole-allowed transitions from the ground $X0_g^+$ state. The spontaneous decay rate of the 0_u^+ state near the dissociation limit is about twice that of the $^1P_1$ atomic state, and the radiative lifetime of the $^1P_1$ state is 5.46 ns [21]. This short lifetime precludes discrimination of the $X0_g^+$-0_u^+ fluorescence from scattered light of the excitation laser pulse. For emission from near-dissociation vibrational levels of the 0_u^+ state, the wavelengths of the fluorescence and the scattered light are too close to be easily distinguished with a monochromator or a spectral filter.

Nevertheless, we have observed emission from $^3P_1$ state atoms, which is caused by photoassociation and the subsequent decomposition process. Because this atomic state has a lifetime of 0.87 μs [37], and because the wavelength of the $^1S_0$-$^3P_1$ transition is 555.6 nm, the fluorescence can be clearly distinguished from the scattered light. Here, the fluorescence was introduced to a monochromator fixed at 555.6 nm, and detected by a photomultiplier tube. The directions of the Yb vapor beam, the excitation laser beam, and the fluorescence collected are all perpendicular to each other. In the measurements of Fig. 2, Fig. 3(b), and those of the $^1S_0$-$^1P_1$ excitation of Fig. 3(a) and Fig. 4(a), an interference spectral filter was used instead of the monochromator. The full width at half maximum (FWHM) of the transmission of the monochromator was 3 nm. The interference filter had the center wavelength of 560 nm and the FWHM of 10 nm. It was confirmed that both instruments gave the same spectral profile of the observed red wing. The signal from the photomultiplier was amplified and then recorded through a digital oscilloscope. All wavelengths described in this paper are the values in a vacuum.

III. RESULT

The observed excitation spectrum is shown in Fig. 2. It is composed of sharp discrete lines and an asymmet-

ric continuous band. The discrete lines correspond to two-photon excitations to atomic Rydberg states. These excitations are enhanced by the near-resonant intermediate $^1P_1$ state. An extensive list of energy levels and assignments of Rydberg states can be seen in Ref. [38], including most of the discrete lines observed here. It is worth noting that, when the excitation laser beam was focused at the observation point, each Rydberg line profile had a tail towards the $^1S_0$-$^1P_1$ line at 398.91 nm. This was attributed to Fano resonance with a photoionization process for a high laser intensity [39].

At low temperatures only the Rydberg lines are observed. This result ensures that small branching for the radiative decay of the $^1P_1$ atomic state to triplet states causing the fluorescence from the $^3P_1$ state [40] is negligible in the present experiment. When the temperature is increased, the $^1S_0$-$^1P_1$ line with a long red wing appears. This wing corresponds to photoassociation, and is visible at wavelengths up to about 402 nm. Figure 3(a) shows the temperature dependence of these spectral components. It also shows that the Rydberg line signal is proportional to the atomic density n in the furnace estimated from the temperature, while the photoassociation signal is proportional to n^2. This behavior supports our association of the red wing with photoassociation, since photoassociation is a two-body collision process. The scattering matrix for a photoassociation collision has been formulated in Ref. [41].

It should be noted that Yb_2 molecules in the $X0_g^+$ ground state are also expected to exist in the vapor, and that their density is approximately proportional to n^2 as explained by the law of mass action [42]. From the vapor pressure of Yb [43] and the potential curve of the $X0_g^+$ state [29], the density of Yb_2 in the furnace is estimated to be 10^8 cm^{-3} at 800 K. To confirm that the red wing corresponds not to bound-bound transitions of Yb_2 but to photoassociation, we assessed the dependence of the signal intensities on the distance from the aperture of the furnace to the excitation point. If the red wing were due to bound-bound transitions, the intensity ratio of the red wing to the Rydberg line would be independent of the distance, since the density ratio of molecules to atoms should not change during free flight from the aperture. Instead, we have confirmed that the intensity ratio decreases as the distance increases. This is consistent with the expectation that atomic density decreases with increasing distance and that the photoassociation signal is proportional to the square of the atomic density at the excitation point. We have also confirmed that the observed spectrum is markedly different from the calculated excitation spectrum of Yb_2 as the sum of all the bound-bound $X0_g^+$-0_u^+ transitions for a thermal population distribution among rovibrational states. Whereas the calculated spectrum increases with increasing wavelength from the $^1S_0$-$^1P_1$ atomic line, the observed spectrum behaves in just the opposite manner.

Figure 3(b) shows the laser pulse energy dependence of the photoassociation and Rydberg line signals in a low

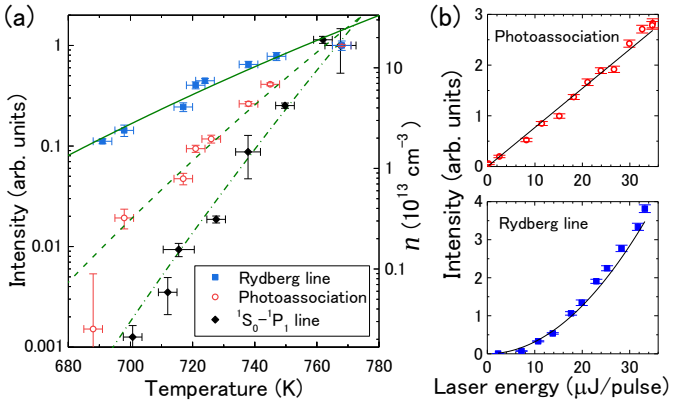

FIG. 3. Temperature and laser energy dependence. (a) Time-integrated fluorescence signal intensities as functions of the temperature of the furnace (dots). These values are normalized to the data points at 768 K. The photoassociation signal is integrated in the range of 399.11-399.21 nm. The excitation laser pulse energy is about 0.2 mJ. The solid line overlaid near the Rydberg line data is the saturated atomic density n in the furnace. Note that the atomic density at the excitation point is about three orders of magnitude smaller than n. The dashed and dot-dashed lines near the photoassociation and the $^1S_0$-$^1P_1$ line data, shown here for informational purposes, are proportional to n^2 and n^3, respectively. (b) Excitation laser energy dependence of the signals (dots). They are well fitted by a straight line for the photoassociation and a quadratic curve for the Rydberg line (lines). The photoassociation signal is taken at 752 K and at 399.20 nm. The Rydberg line signal is at 626 K and at 398.96 nm, and corresponds to the transition to the $6s23s$ $^1S_0$ state.

pulse energy range. The Rydberg line shows a quadratic behavior with respect to the laser energy, while the photoassociation shows a linear behavior. These results confirm that the sharp lines are two-photon excitations to Rydberg states and that the red wing assigned to the photoassociation is a one-photon excitation.

Figure 4 shows the time profiles of fluorescence signals of the Rydberg line, the $^1S_0$-$^1P_1$ line, and photoassociation. As shown in Fig. 4(a), the rise and fall times of the profiles become long at high temperatures. This behavior can be explained as radiation trapping, i.e., the repeated absorption and re-emission of the 555.6 nm photons (and also 398.9 nm photons for the $^1S_0$-$^1P_1$ line) by surrounding atoms due to high atomic density. The profiles at 728 K in Fig. 4(a) and that at 738 K in Fig. 4(b) are confirmed to be the same with those at lower temperatures, which means that the radiation trapping is negligible for these profiles. The Rydberg line signal has longer rise and fall times than the photoassociation signal has, because this $6s20s$ $^1S_0$ Rydberg state has a long radiative lifetime of 0.65 μs [44] and can decay both directly and indirectly to the $^3P_1$ state. The fall times of both signals mainly reflect the radiative lifetime of 0.87 μs of the $^3P_1$ state.

A remarkable feature is the rise time of the photoas-

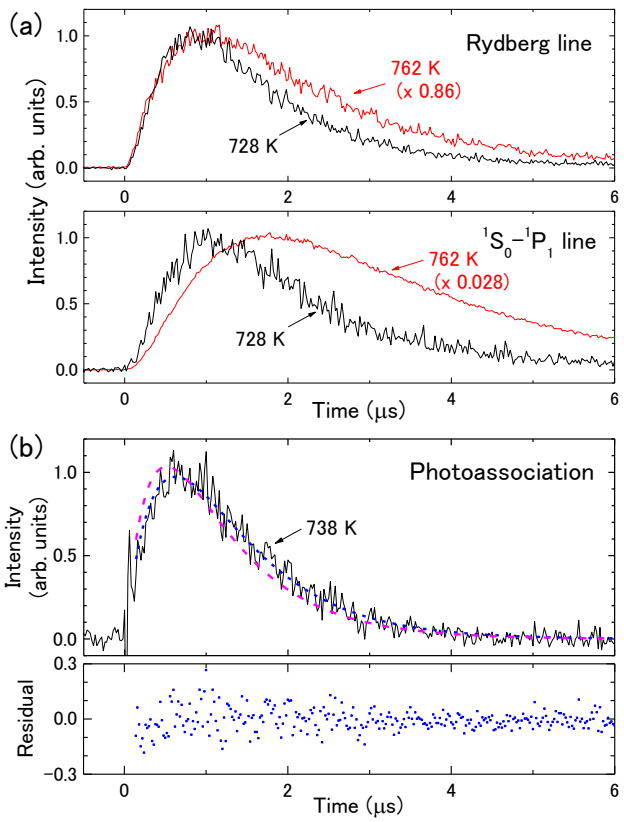

FIG. 4. Time profiles of observed fluorescence signals. The time origin is irradiation of the excitation laser pulse. (a) Profiles of a Rydberg line and the $^1S_0$-$^1P_1$ line. The Rydberg line is the transition to the $6s20s$ $^1S_0$ state at 399.99 nm. The signal intensity for the higher temperature in each panel is multiplied by 0.86 for the Rydberg line and 0.028 for the $^1S_0$-$^1P_1$ line to give the same peak height with the lower temperature profile. (b) Profile of photoassociation taken with the excitation at 399.20 nm. The dot-dashed and dashed lines in the upper panel are fitted curves of Eq. (2) with $(1/\kappa_2, 1/\gamma) =$ (0.33, 0.87) μs and (0.46, 0.87) μs, respectively (see, Sec. IV), where the fitting parameter is only the amplitude A. The residual from the dashed line is also shown in the lower panel.

sociation signal, which is much longer than the radiative lifetime of the 0_u^+ state. Note that the response time of the photon detection system is about 20 ns, which is negligibly shorter than this rise time. This result indicates that the $^3P_1$ state atoms are not directly produced from the 0_u^+ state. If the production of the $^3P_1$ state atoms were a direct one-step process with a rate κ, the time profile would fit the solution

$$N_1 = A[e^{-\gamma t} - e^{-(\Gamma+\kappa)t}], \qquad (1)$$

of rate equations $dN_0/dt = -(\Gamma+\kappa)N_0$, $dN_1/dt = \kappa N_0 - \gamma N_1$. Here, A is a fitting parameter related to the number of initial 0_u^+ state molecules, t is time, and N_0 and N_1 are the numbers of molecules in the 0_u^+ state and atoms in the $^3P_1$ state, respectively. The rates Γ and γ are the inverses of the radiative lifetimes of the 0_u^+ state and the $^3P_1$ state, and are 0.37 GHz and 1.1 MHz, respectively. However, the large value of Γ does not allow Eq. (1) to realize the observed long rise time of the photoassociation signal. Therefore, at least one more step is needed in the decay process from the 0_u^+ state to the $^3P_1$ state with a decay time of several hundred nanoseconds.

In the end, we briefly mention the experimental results for excitation at the $^1S_0$-$^1P_1$ atomic resonance and at its tail in the blue side. The temperature dependence of the $^1S_0$-$^1P_1$ line shown in Fig. 3(a) indicates that the signal intensity is proportional to n^3, which means that three-body collisions are responsible for the production of the $^3P_1$ state atoms. The time profile of the $^1S_0$-$^1P_1$ line shown in Fig. 4(a) extends to much longer time than the radiative lifetime of the $^1P_1$ state. This result indicates that the $^3P_1$ state atoms are not directly produced from the $^1P_1$ state atoms. The spectral tail in the blue side, which is less pronounced than the red wing as shown in Fig. 2, is explained as the power-broadened tail of the $^1S_0$-$^1P_1$ atomic resonance. The spectral profile around the peak and of the blue tail is well fitted by a Lorentzian function with the FWHM of 5×10^{-3} nm, which is a reasonable value compared with the excitation laser pulse intensity. The temperature dependence and the time profile of excitation at 398.87 nm, which is on the blue tail, are similar to those of the $^1S_0$-$^1P_1$ line.

IV. DECAY PROCESS

Production of the $^3P_1$ state atoms in the case of photoassociation is due to predissociation of the 0_u^+ state molecules. However, predissociation of the 0_u^+ state with states correlating to the $^1S_0$+^3P states, which may occur at short internuclear distances and has been theoretically discussed in Ref. [45], cannot be responsible for the observed fluorescence. Direct dissociation to the $^1S_0$+$^3P_1$ state cannot explain the long rise time in Fig. 4(b), and dissociation to the $^1S_0$+$^3P_{0,2}$ states does not lead to production of the $^3P_1$ state atoms. The long rise time of the photoassociation signal suggests a two-step decay process consisting of predissociation of the 0_u^+ state with the $^1S_0$+^3D states followed by radiative decay of the ^3D-$^3P_1$ transitions, as shown in Fig. 5. The $^3D_1$ and $^3D_2$ atomic levels are located at 579 cm^{-1} and 316 cm^{-1} from the $^1P_1$ level as shown in Fig. 1(b), respectively. The radiative lifetimes of the $^3D_1$ and $^3D_2$ states are 0.33 μs [37] and 0.46 μs [46], which are long enough to explain the rise time. The $^3D_{1,2}$ states mostly decay to the ^3P states. The decay rates from the $^3D_1$ and $^3D_2$ states to the $^3P_1$ state are 1 MHz and 2 MHz, respectively [47].

Since the total decay rate $\Gamma+\kappa_1$ of the 0_u^+ state is very large, the time profile of the fluorescence signal in a long time scale can be expressed similarly to Eq. (1) as

$$N_1 = A(e^{-\gamma t} - e^{-\kappa_2 t}), \qquad (2)$$

where κ_2 represents the inverse of the radiative lifetime of the ^3D states. The dot-dashed and dashed lines in

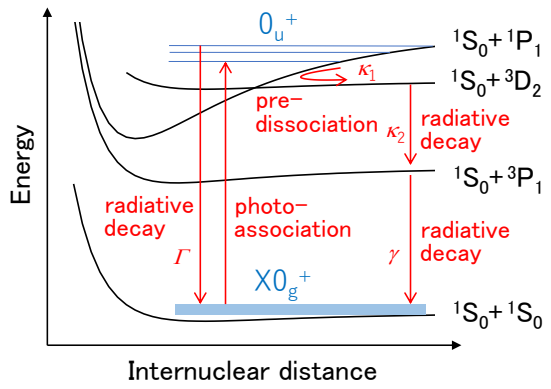

FIG. 5. Schematic for the suggested decay process of the 0_u^+ state.

Fig. 4(b) show the expected profiles for dissociation to the $^1S_0$+$^3D_1$ and $^1S_0$+$^3D_2$ states, respectively. The result for the $^1S_0$+$^3D_2$ state is in good agreement with the observed profile at 738 K. From this agreement the dissociation channel is identified to be the $^1S_0$+$^3D_2$ state.

In the case of excitation at the $^1S_0$-$^1P_1$ line, not only the 0_u^+ state but also the long-lived 1_g state is expected to be populated via three-body collisions. The rise time of the fluorescence signal of the $^1S_0$-$^1P_1$ line in Fig. 4(a), which is longer than that of the photoassociation signal, can be explained by the involvement of the 1_g state molecules.

V. PREDISSOCIATION LINEWIDTH

Previous photoassociation studies on ultracold Yb atoms [21, 23] have reported vibrational-level dependent line broadening. Unpublished data obtained by Ref. [23] for the linewidths of the photoassociation is shown in Fig. 6. The linewidth should be the sum of the predissociation width and the radiative decay width $\Gamma/2\pi$. It begins to broaden at vibrational levels about 8 cm^{-1} from the dissociation limit. The observed predissociation is caused by the homogeneous spin-orbit interaction [48] that occurs with heavy dimers such as Yb_2. Heterogeneous interactions [48], which become stronger as the rotational angular momentum increases, are too weak to explain the linewidth broadening seen in Fig. 6 for the photoassociation from the $J''=0$ state with J'' the rotational angular momentum of the $X0_g^+$ state. This homogeneous interaction couples the 0_u^+ state with a 0_u state correlating to the $^1S_0$+$^3D_2$ state.

In the following, the bound 0_u^+ state and the dissociating 0_u state are referred to $|\mathrm{e}\rangle$ and $|\mathrm{d}\rangle$, respectively. The predissociation is caused by a potential crossing between these states. The potential curve of $|\mathrm{e}\rangle$ is well expressed by the asymptotic form of $V_\mathrm{e}(r) = -C_{3\mathrm{e}}/r^3 - C_{6\mathrm{e}}/r^6$ at long r. The potential coefficients are $C_{3\mathrm{e}} = 11.535$ a.u. and $C_{6\mathrm{e}} = 1.2\times10^3$ a.u. [23]. The short-range theoretical potential curve of $|\mathrm{e}\rangle$ shown in Fig. 1(a) is connected to this long-range curve. The potential curve of $|\mathrm{d}\rangle$ is much flatter at long r because its asymptotic form is $C_{5\mathrm{d}}/r^5 - \epsilon$ [49], where ϵ is the energy difference between the $^1P_1$ and $^3D_2$ atomic levels. These two potential curves are expected to intersect at about $r_\mathrm{c} = 1.1$ nm, which is fairly long.

In such a case of the potential crossing at the outer turning point of $|\mathrm{e}\rangle$, the predissociation linewidth $\kappa_1/2\pi$ is expected to undulate as a function of the vibrational energy level E_v. The predissociation linewidth at E_v is given by $2\pi|H_{\mathrm{ed}}(r_\mathrm{c})|^2|\langle\psi_\mathrm{e}(E_v)|\psi_\mathrm{d}(E_v)\rangle|^2$, where $H_{\mathrm{ed}}(r_\mathrm{c})$ represents the electronic interaction between $|\mathrm{e}\rangle$ and $|\mathrm{d}\rangle$ at r_c, and $|\langle\psi_\mathrm{e}(E_v)|\psi_\mathrm{d}(E_v)\rangle|^2$ is the Franck-Condon factor with the continuum wave function $\psi_\mathrm{d}(E_v)$ being energy-normalized [48]. Dominant contribution to the Franck-Condon factor comes from a region around the potential crossing. The relative phase $\phi(E_v)$ at r_c between the radial wave functions $\psi_\mathrm{e}(E_v)$ and $\psi_\mathrm{d}(E_v)$ is important, and the dependency of the linewidth on $\phi(E_v)$ is given by $\sin^2[\phi(E_v)+\pi/4]$ [48, 50]. The relative phase $\phi(E_v)$ is given by

$$\phi(E_v) = \frac{\sqrt{2\mu}}{\hbar}\Big[\int_{a_\mathrm{e}}^{r_\mathrm{c}} dr\sqrt{E_v - V_\mathrm{e}(r)} - \int_{a_\mathrm{d}}^{r_\mathrm{c}} dr\sqrt{E_v - V_\mathrm{d}(r)}\,\Big], \tag{3}$$

where μ is the reduced mass, $\hbar$ is the Planck constant divided by 2π, and a_e and a_d are the inner turning points of $V_\mathrm{e}(r)$ and $V_\mathrm{d}(r)$ at E_v, respectively.

The range of E_v of our interest is $-25 < E_v < -2$ cm^{-1} for the comparison of the linewidths of Ref. [23]. The first term of Eq. (3) varies monotonically by about 5 rad in this range. Although no information on $V_\mathrm{d}(r)$ is available, the second term should behave similarly to the first term and the amount of the change should be on the same order. Thus, the revival of the narrow photoassociation linewidth is expected at not so large detuning because of the undulation of the linewidth. An example of the calculated result for a simple hard-core potential, $V_\mathrm{d}(r) = \infty$ for $r < a_\mathrm{d}$ and $V_\mathrm{d}(r) = -\epsilon$ for $r \geq a_\mathrm{d}$, is shown in Fig. 6, where the observed linewidths are nicely reproduced and narrow linewidths are recovered at about -21 cm^{-1}.

VI. SPECTRUM CALCULATION

Next, the observed red wing is compared with a theoretical excitation spectrum of the photoassociation to the 0_u^+ state for a $^{174}Yb_2$ homonuclear atomic pair. Since the red wing is located near the $^1S_0$-$^1P_1$ atomic line, it is generated primarily due to transitions between the $^1S_0$+$^1S_0$ scattering states with low collision energies and high vibrational states near the dissociation limit of the 0_u^+ state. Note that, at near-dissociation levels, properties such as vibrational level spacings are insensitive to the short-range potential curve, and thus the calculated spectrum is almost independent of the short-range

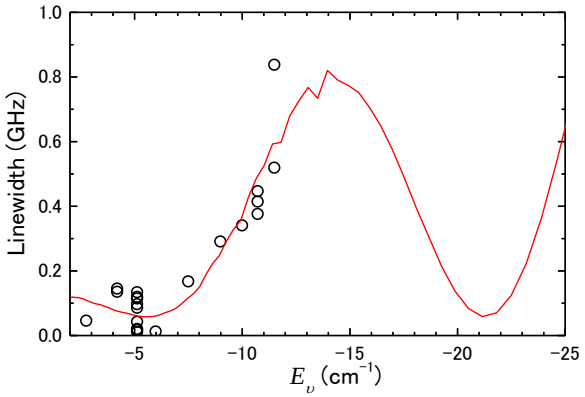

FIG. 6. Linewidths of vibrationally resolved photoassociation transitions from the $J'' = 0$ s-wave scattering state obtained in a previous study on ultracold atoms [23] (circles). The uncertainties of the linewidths are typically 0.05 GHz. The line shows an example of calculated linewdths $(\kappa_1 + \Gamma)/2\pi$ for a hard-core potential with the parameters $a_{\rm d} = 0.353$ nm and $H_{\rm ed}(r_{\rm c}) = 4.3$ cm^{-1}. The vibrational level E_v is measured from the $^1S_0$+$^1P_1$ dissociation limit.

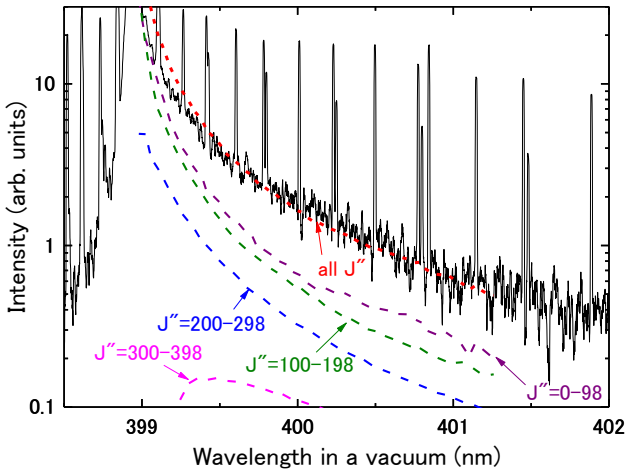

FIG. 7. Comparison of an observed spectrum at 764 K (solid line) with calculated excitation spectra (dashed lines) of the photoassociation for various ranges of J''. There is no fitting parameter in the calculated spectrum except its total amplitude.

potential. The potential curve $V_{\rm e}(r)$ of the 0_u^+ state is described in the previous section. The ground state potential $V_{\rm g}(r)$ is taken from Ref. [29], where the *ab initio* potential of Ref. [16] is smoothly connected to the asymptotic form of $-C_{6{\rm g}}/r^6 - C_{8{\rm g}}/r^8$ with adequate scaling to reproduce two-color photoassociation spectra. The well depth of $V_{\rm g}(r)$ is 743 cm^{-1}, and the coefficients are $C_{6{\rm g}} = 1933.5$ a.u. and $C_{8{\rm g}} = 2.172 \times 10^5$ a.u. [29]. Transition strength is obtained for each transition between an energy-normalized scattering state of even J'' in the $X0_g^+$ state and a unit-normalized bound state of an odd rotational angular momentum J' in the 0_u^+ state by calculating the Franck-Condon and Hönl-London factors. The electronic transition dipole moment is assumed to be independent of r. We have focused on a range of detuning from the $^1S_0$-$^1P_1$ line within 150 cm^{-1}. The corresponding wavelengths range up to 401.3 nm. At $V_{\rm e}(r) = -150$ cm^{-1} with $r = 1.4$ nm, the contribution of the $C_{6{\rm e}}/r^6$ term is still only 0.6% , and thus the potential is well expressed by the asymptotic form. The relative kinetic energy E of the scattering state is considered up to 150 cm^{-1} (= 216 K) in the calculation. The population distribution among the scattering states is deduced by considering the relative motion of a pair of atoms in an effusive atomic beam as described in Appendix A. The ground state potential does not support bound states for $J'' > 282$ due to the centrifugal term. The quasibound states inside the centrifugal barrier for the $X0_g^+$ state are neglected, because most of them are confined within short internuclear distances such that the Franck-Condon factors for near-dissociation levels are small. The quasibound states of the 0_u^+ state, on the other hand, are taken into account, since the barrier is located at relatively long r due to the r^{-3} dependence of $V_{\rm e}(r)$.

The calculated spectrum is shown in Fig. 7 along with the observed spectrum in a semi-log scale. The contribution from various ranges of J'' is also shown. Note that the contribution from the $J'' > 400$ states is negligibly small. The observed red wing is well reproduced by the calculated excitation spectrum. This good agreement supports the assignment of the red wing to the photoassociation to the 0_u^+ state. This comparison of the observed and calculated spectra is under the assumption that the predissociation rate κ_1 is much larger than the radiative decay rate Γ. Although the predissociation rate κ_1 is strongly dependent on the vibrational level, it is often much larger than the radiative lifetime Γ as shown in Fig. 6 as the calculated example and its undulation is averaged out by the contribution from various values of J'' and E. Thus, this simplification of the predissociation rate is a reasonable assumption for this comparison.

VII. CONCLUSION

The continuous excitation spectrum of hot Yb vapors observed as a red wing of the $^1S_0$-$^1P_1$ atomic line at 399 nm is assigned to photoassociation to the 0_u^+ molecular state. This assignment is supported by the agreement between the observed and calculated excitation spectra, the dependence on atomic density, and the dependence on the distance of the excitation point from the furnace. The photoassociation causes fluorescence from the $^3P_1$ state atoms, which enables sensitive detection of the production of Yb_2 molecules. The long rise time of the fluorescence signal suggests that the $^3P_1$ state atoms are produced by a two-step process consisting of predissociation of the 0_u^+ state with the $^1S_0$+$^3D_2$ state and subsequent

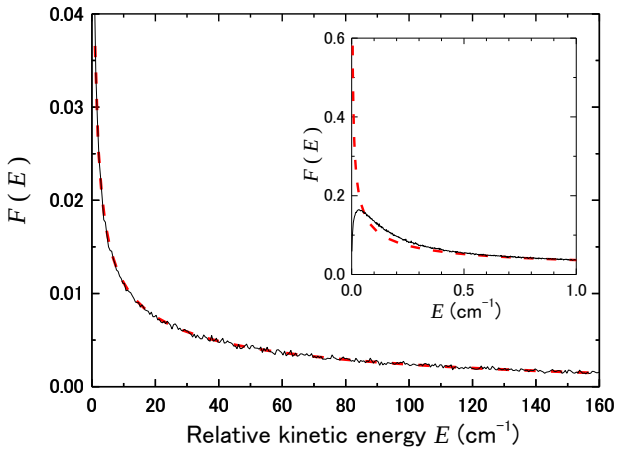

FIG. 8. Simulated relative kinetic energy distribution for collisions of ^{174}Yb atoms in an effusive beam (solid line) and the distribution function of Eq. (A4) (dashed line). The inset shows a magnified graph near $E = 0$.

radiative decay to the $^1S_0$+$^3P_1$ state. This model can nicely explain the previous observations of the broadening of the photoassociation lines of ultracold atoms, and suggests that narrow photoassociation lines would be recovered at not so large detuning. The comparison of photoassociation linewidths of several isotopes would allow us to determine the relative phase of Eq. (3) through the mass scaling analysis similar to Refs. [24, 29] and to predict linewidths of all the other isotopes.

ACKNOWLEDGEMENTS

We acknowledge W. Kusano, N. Hada, and Y. Makiyama for their assistance with the experiment. We also thank M. Kitagawa, K. Kasa, and S. Tojo for their cooperation in the experiment regarding Fig. 6. This work is supported by JSPS KAKENHI Grant Number JP20K03805 and by the Toray Science Foundation, and is also partially supported by Grants-in-Aid for Scientific Research from JSPS (Nos. JP17H06138, JP18H05405, and JP18H05228), JST CREST (No. JP-MJCR1673), and the MEXT Quantum Leap Flagship Program (MEXT Q-LEAP) Grant No. JPMXS0118069021.

Appendix A: RELATIVE MOTION IN AN EFFUSIVE BEAM

A photoassociation rate coefficient is obtained from the scattering matrix element $S_{0,ia}$ given in Ref. [41] averaged over the energy distribution $F(E)$ of relative motion of a colliding atom pair as [51],

$$\int_0^\infty dE F(E) \frac{\pi \upsilon_{\rm rel}}{k^2} \sum_{J''} (2J''+1)|S_{0,ia}|^2, \qquad \text{(A1)}$$

where $\upsilon_{\rm rel}$ is the relative velocity, and $k = \sqrt{2\mu E}/\hbar$. For example, the energy distribution of relative motion of a pair of atoms in the Maxwell-Boltzmann distribution is

$$F(E) = \frac{2}{\sqrt{\pi}} (\frac{1}{k_B T})^{\frac{3}{2}} \sqrt{E} \exp(-\frac{E}{k_B T}), \qquad \text{(A2)}$$

where k_B is the Boltzmann constant, and T is the temperature.

In the present experiment, photoassociation in an effusive beam is investigated. The distribution of the relative kinetic energy in this situation is considerably different from Eq. (A2). The velocity distribution of an atom in an effusive beam is given by,

$$f(v) = \frac{4}{\pi} (\frac{m}{2k_B T})^{\frac{3}{2}} v^2 \exp(-\frac{m}{2k_B T} v^2), \qquad \text{(A3)}$$

where m is the mass of the atom, and v is the velocity. When the distance L of the excitation point from the aperture of the furnace is much larger than the aperture diameter d, a collision between a pair of atoms flying to the same direction should be considered. From integration of $f(v)f(v-\upsilon_{\rm rel})$, the relative kinetic energy distribution of a pair of atoms of an identical mass is obtained as,

$$F(E) = \frac{(3-2x)e^{-2x}}{\pi k_B T} + \frac{(4x^2-4x+3)\mathrm{erfc}(\sqrt{x})e^{-x}}{\pi k_B T \sqrt{x}}, \qquad \text{(A4)}$$

where $x = E/k_B T$ and $\mathrm{erfc}(t) = \int_t^\infty dt \exp(-t^2)$. This energy distribution is not applicable to very small E, because the relative velocity component vertical to the direction of the flight is not negligible in this case. A simulation result of the energy distribution is shown in Fig. 8. The parameters assumed are $L = 20$ mm, $d = 1$ mm, and $T = 764$ K. The simulation agrees excellently with Eq. (A4) except a region of very small E. The calculated spectrum of Fig. 7 is obtained with this simulated energy distribution.

[1] S. Taie, R. Yamazaki, S. Sugawa, and Y. Takahashi, Nat. Phys. **8**, 825830 (2012).
[2] S. Nakajima, T. Tomita, S. Taie, T. Ichinose, T. Ozawa, L. Wang, M. Troyer, and Y. Takahashi, Nat. Phys. **12**, 296300 (2016).
[3] W.F. McGrew *et al.*, Nature **564**, 87 (2018).
[4] M. Pizzocaro, F. Bregolin, P. Barbieri, B. Rauf, F. Levi, and D. Calonico, Metrologia **57**, 035007 (2020).
[5] L. Luo *et al.*, Metrologia **57**, 065017 (2020).
[6] T. Kobayashi *et al.*, Metrologia **57**, 065021 (2020).

[7] T. Bergeman and P.F. Liao, J. Chem. Phys. **72**, 886 (1980).

[8] G. Gerber, R. Möller, and H. Schneider, J. Chem. Phys. **81**, 1538 (1984).

[9] C. Bordas, M. Broyer, J. Chevaleyre, and P. Dugourd, Chem. Phys. Lett. **197**, 562 (1992).

[10] A. Stein, H. Knöckel, and E. Tiemann, Phys. Rev. A **78**, 042508 (2008).

[11] A. Stein, H. Knöckel, and E. Tiemann, Eur. Phys. J. D **57**, 171 (2010).

[12] A. Stein, H. Knöckel, and E. Tiemann, Eur. Phys. J. D **64**, 227 (2011).

[13] M.A. Lebeault, J. Viallon, V. Boutou, and J. Chevaleyre, J. Mol. Spectrosc. **192**, 179 (1998).

[14] S. Suzer and L. Andrews, J. Chem. Phys. **89**, 5514 (1988).

[15] Y. Wang and M. Dolg, Theor. Chem. Acc. **100**, 124 (1998).

[16] A.A. Buchachenko, G. Chałasiński, and M.M. Szczęśniak, Eur. Phys. J. D **45**, 147 (2007).

[17] N.S. Mosyagin, A.N. Petrov, and A.V. Titov, arXiv:0901.0077v6 (2009).

[18] S.G. Porsev, M.S. Safronova, A. Derevianko, and C.W. Clark, Phys. Rev. A **89**, 012711 (2014).

[19] P. Tecmer, K. Boguslawski, M. Borkowski, P.S. Żuchowski, and D. Kedziera, Int. J. Quant. Chem. **119**, e25983 (2019).

[20] J.J. Lutz and J.M. Hutson, J. Mol. Spectrosc. **330**, 43 (2016).

[21] Y. Takasu, K. Komori, K. Honda, M. Kumakura, T. Yabuzaki, and Y. Takahashi, Phys. Rev. Lett. **93**, 123202 (2004).

[22] S. Tojo, M. Kitagawa, K. Enomoto, Y. Kato, Y. Takasu, M. Kumakura, and Y. Takahashi, Phys. Rev. Lett. **96**, 153201 (2006).

[23] K. Enomoto, M. Kitagawa, K. Kasa, S. Tojo, and Y. Takahashi, Phys. Rev. Lett. **98**, 203201 (2007).

[24] M. Kitagawa, K. Enomoto, K. Kasa, Y. Takahashi, R. Ciuryło, P. Naidon, and P.S. Julienne, Phys. Rev. A **77**, 012719 (2008).

[25] K. Enomoto, M. Kitagawa, S. Tojo, and Y. Takahashi, Phys. Rev. Lett. **100**, 123001 (2008).

[26] M. Borkowski, R. Ciuryło, P. S. Julienne, S. Tojo, K. Enomoto, and Y. Takahashi, Phys. Rev. A **80**, 012715 (2009).

[27] M. Borkowski, R. Ciuryło, P. S. Julienne, R. Yamazaki, H. Hara, K. Enomoto, S. Taie, S. Sugawa, Y. Takasu, and Y. Takahashi, Phys. Rev. A **84**, 030702(R) (2011).

[28] Y. Takasu, Y. Saito, Y. Takahashi, M. Borkowski, R. Ciuryło, and P.S. Julienne, Phys. Rev. Lett. **108**, 173002 (2012).

[29] M. Borkowski, A.A. Buchachenko, R. Ciuryło, P.S. Julienne, H. Yamada, Y. Kikuchi, K. Takahashi, Y. Takasu, and Y. Takahashi, Phys. Rev. A **96**, 063405 (2017).

[30] J.H. Han, J.H. Kang, M. Lee, and Y. Shin, Phys. Rev. A **97**, 013401 (2018).

[31] O. Bettermann, N. Darkwah Oppong, G. Pasqualetti, L. Riegger, I. Bloch, and S. Fölling, arXiv:2003.10599v1 (2020).

[32] H. Wang, P.L. Gould, and W.C. Stwalley, Phys. Rev. Lett. **80**, 476 (1998).

[33] N. Allard and J. Kielkopf, Rev. Mod. Phys. **54**, 1103 (1982).

[34] G. Herzberg, *Molecular Spectra and Molecular Structure Vol. I - Spectra of Diatomic Molecules*, (Van Nostrand, 1950).

[35] K. Ueda, O. Sonobe, H. Chiba, and Y. Sato, J. Chem. Phys. **95**, 8083 (1991).

[36] K. Ueda, H. Chiba, and Y. Sato, Phys. Rev. A **45**, 2090 (1992).

[37] K. Beloy, J.A. Sherman, N.D. Lemke, N. Hinkley, C.W. Oates, and A.D. Ludlow, Phys. Rev. A **86**, 051404(R) (2012).

[38] M. Aymar, A. Débarre, and O. Robaux, J. Phys. B: At. Mol. Opt. Phys. **13**, 1089 (1980).

[39] L. Armstrong, Jr., B.L. Beers, and S. Feneuille, Phys. Rev. A **12**, 1903 (1975).

[40] K. Honda, Y. Takahashi, T. Kuwamoto, M. Fujimoto, K. Toyoda, K. Ishikawa, and T. Yabuzaki, Phys. Rev. A **59**, R934 (1999).

[41] J.L. Bohn and P.S. Julienne, Phys. Rev. A **60**, 414 (1999).

[42] D. Budker, D.F. Kimball, and D.P. DeMille, *Atomic Physics: An Exploration Through Problems and Solutions* (Oxford University Press, 2008).

[43] C.E. Habermann and A.H. Daane, J. Chem. Phys. **41**, 2818 (1964).

[44] W. Dadi, W. Chengfei, and J. Zhankui, J. Phys. B: At. Mol. Phys. **20**, L555 (1987).

[45] M. Machholm, P.S. Julienne, and K.-A. Suominen, Phys. Rev. A **64**, 033425 (2001).

[46] C.J. Bowers, D. Budker, E.D. Commins, D. DeMille, S.J. Freedman, A.-T. Nguyen, S.-Q. Shang, and M. Zolotorev, Phys. Rev. A **53**, 3103 (1996).

[47] S.G. Porsev, Y.G. Rakhlina, and M.G. Kozlov, Phys. Rev. A **60**, 2781 (1999).

[48] H. Lefebvre-Brion and R.W. Field, *The Spectra and Dynamics of Diatomic Molecules*, (Elsevier, 2004).

[49] J. Mitroy and J.-Y. Zhang, Phys. Rev. A **76**, 062703 (2007).

[50] D.S. Ramsay and M.S. Child, Mol. Phys. **22**, 263 (1971).

[51] K.M. Jones, E. Tiesinga, P.D. Lett, and P.S. Julienne, Rev. Mod. Phys. **78**, 483 (2006).